

## RESEARCH ARTICLE

# Numerical investigation of the influence of the source and detector position for optical measurement of lung volume and oxygen content in preterm infants

Andrea Pacheco<sup>1,2\*</sup>  | Baptiste Jayet<sup>1</sup> | Emilie Krite Svanberg<sup>3</sup> |  
Hamid Dehghani<sup>4</sup> | Eugene Dempsey<sup>5</sup> | Stefan Andersson-Engels<sup>1,2</sup>

<sup>1</sup>Biophotonics@Tyndall, IPIC, Tyndall National Institute, Cork, Ireland

<sup>2</sup>Department of Physics, University College Cork, Cork, Ireland

<sup>3</sup>Department of Clinical Sciences, Paediatric Anaesthesiology and Intensive Care Medicine, Skåne University Hospital, Lund University, Lund, Sweden

<sup>4</sup>School of Computer Science, the University of Birmingham, Birmingham

<sup>5</sup>INFANT Centre, Cork University Maternity Hospital, University College Cork, Ireland

## \*Correspondence

Andrea Pacheco, Tyndall National Institute, Lee Maltings, Dyke Parade, T12R5CP Cork, Ireland.  
Email: andrea.pacheco@tyndall.ie

## Funding information

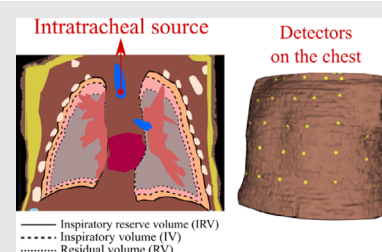
Science Foundation Ireland, Grant/Award Number: SFI/15/RP/2828

## Abstract

There is an urgent need for improved respiratory surveillance of preterm infants. Gas in scattering media absorption spectroscopy (GASMAS) is emerging as a potential clinical cutaneous monitoring tool of lung functions in neonates. A challenge in the clinical translation of GASMAS is to obtain sufficiently high signal-to-noise ratios in the measurements, since the light attenuation is high in human tissue. Previous GASMAS studies on piglets have shown higher signal quality with an internal source, as more light propagates through the lung and the loss due to scattering and absorption is less. In this article we simulated light propagation with an intratracheal and a dermal source, and investigated the signal quality and lung volume probed. The results suggest that GASMAS has the potential to measure respiratory volumes; and the sensitivity is higher for an intratracheal source which also enables to probe most of the lung.

## KEYWORDS

computational model of a thorax, light transport, preterm infants, tuneable diode laser absorption spectroscopy



## 1 | INTRODUCTION

Prematurity is the leading cause of neonatal mortality worldwide. In 2010, the estimated mean preterm birth rate was between 12.3% and 18.1%, resulting in 14.9 million infants born before 37 weeks of gestation worldwide [1]. Premature birth can result in long-term

complications and the associated health-risks increase with lower gestational age [2].

The lungs of preterm infants lack both structural and biochemical maturation, which together with surfactant (lipoprotein decreasing surface tension in the alveoli) deficiency and incomplete vascularization can cause respiratory distress syndrome (RDS) [3]. RDS in turn

This is an open access article under the terms of the Creative Commons Attribution-NonCommercial-NoDerivs License, which permits use and distribution in any medium, provided the original work is properly cited, the use is non-commercial and no modifications or adaptations are made.

© 2022 The Authors. *Journal of Biophotonics* published by Wiley-VCH GmbH.

results in respiratory failure manifested by a lack of oxygen and excess of carbon dioxide. The clinical criteria for RDS diagnosis include fast shallow breathing (tachypnea), blueish skin (cyanosis), chest retractions, flaring nostrils and expiratory grunting sounds [4]. Chest radiography shows a ground-glass appearance, air bronchograms and hypo-expansion of the lungs; pulse oximetry may show low level of oxygen and blood gas analysis an accumulation of carbon dioxide in the blood [5].

Antenatal administration of corticosteroids, nasal continuous positive airway pressure (NCPAP) and surfactant administration to preterm neonates reduce the severity of RDS and minimise further development of respiratory disease [5, 6]. These therapies alongside invasive mechanical ventilation aim to achieve optimal lung volumes. However, excessive inspiratory pressures represent a risk for baro-traumatic lung injury and long term problems such as chronic lung disease [7].

Gas in scattering media absorption spectroscopy (GASMAS) is a tuneable diode laser spectroscopic technique developed for noninvasive measurement of gas enclosed inside turbid media without extraction [8]. The technique relies on the sharp and specific absorption lines of gases, enabling sensitive measurements of gas concentrations in the presence of a scattering solid-state media with much broader absorption features [9, 10]. GASMAS has industrial applications including quality control and characterisation of wood, food packaging, ceramics and pharmaceutical tablets [11–15]; further studies are addressing its clinical translation for assessment of inflammation and infection in paranasal sinus cavities [16–18], otitis diagnosis [19] and early prediction of osteonecrosis [20]. The application of main relevance for the work in this article is the monitoring of oxygen ( $O_2$ ) and water ( $H_2O$ ) vapour in the lungs of new-born infants [21, 22]. GASMAS is a light-based technology, therefore, it is nonharmful and its clinical applications are contributing to the accomplishment of the UN third Sustainability Development Goal [23].

In a typical GASMAS measurement targeting to sense  $O_2$  content in the lungs of a neonate, a dual wavelength diffuse laser source illuminates the walls of the chest. Light scattered from the inflated alveoli within the lung, reach a photodetector and the attenuated signal from the gas is identified. One of the lasers scans an absorption line of molecular  $O_2$  around 760 nm and the second scans an absorption line of  $H_2O$  vapour around 820 or 934 nm. The wavelengths are spectrally close, and the path length within the tissue is assumed to be approximately the same. The vapour concentration is calculated using the ideal gas law and the Arden Buck equation [24], for known relative humidity and temperature (100%

and  $\sim 37^\circ C$ , respectively). The  $H_2O$  absorption signal is used to estimate the absorption path length by means of the Beer–Lambert law [25].

$$I = I_0 e^{-\epsilon c l} \quad (1)$$

where  $I$  is the intensity of light reaching the detector,  $I_0$  is the intensity of the light source,  $\epsilon$  is the molar absorption of the gas,  $c$  the gas concentration and  $l$  the gas absorption path length.

Consequently, the calculated value of  $l$  is input in Equation (1) to estimate the  $O_2$  concentration, using the absorption signal of light at 760 nm.

Previous study focused in advancing GASMAS for  $O_2$  gas sensing in the lungs of pre-term neonates included theoretical modelling [26], tissue phantom measurements [27–29], and feasibility studies with new-born piglets [30], and healthy full-term infants [22, 31, 32]. Most of these studies have been conducted noninvasively with both source and detector placed on the thorax wall. The results have suggested that stronger signal would be required to gain clinical acceptance.

The quality of the measured gas absorption signal could improve by utilising an internal light source. Severe RDS often need invasive mechanical ventilation, with a tube inserted in the trachea. Almost all preterm infants have a naso-gastric feeding tube, inserted in one nostril, located in the oesophagus and ending in the stomach. An internal light source approach, either through the endotracheal tube or the naso-gastric feeding tube, will potentially provide better signal quality, less light attenuation due to scattering and absorption, and a more robust signal [33].

Larsson et al. found that light administration with a fibre inside the trachea of a phantom model, gives larger gas absorption signals with higher signal-to-noise ratio compared with dermal sources [28]. Krite Svanberg et al. performed measurements in mechanically ventilated piglets with light sources placed in the oesophagus and on the skin, concluding that the detected gas absorption signal is one order of magnitude larger in comparison with measurements taken with a dermal light source [30]. Aiming to fully understand these results, and evaluate the pros and cons of placing an endotracheal and/or dermal source, we in this article, present simulations showing the gain in signal arising from the placement of a light source in the trachea of a computational model from a neonate's thorax. And, based on the results, we highlight the possibility to apply GASMAS technology to sense the changes in pulmonary volume during respiration.

The conducted studies are based on diffuse light modelling implemented with the software package NIRFAST [34]. The geometry of the thorax was recovered

**TABLE 1** Optical properties ( $\mu_a$  and  $\mu_s'$ ) at 760 and 820 nm assigned to the 9 tissue types included in the computational thoracic models

Tissue	760 nm		820 nm		References
	$\mu_a$ (cm <sup>-1</sup> )	$\mu_s'$ (cm <sup>-1</sup> )	$\mu_a$ (cm <sup>-1</sup> )	$\mu_s'$ (cm <sup>-1</sup> )	
Skin	0.031	24.82	0.027	22.76	[10, 35]
Fat	0.128	13.85	0.069	13.24	[36]
Muscle	0.196	14.07	0.198	12.82	[10, 37]
Bone	0.100	9.30	0.110	8.40	[10]
Cartilage	0.532	7.93	0.544	8.46	[38]
Heart	0.249	4.89	0.111	4.45	[10]
Artery	3.138	16.69	4.906	15.87	[10]
Trachea	0.196	14.07	0.198	12.82	[10]
Lung	0.505	5.37	0.740	4.99	[10]

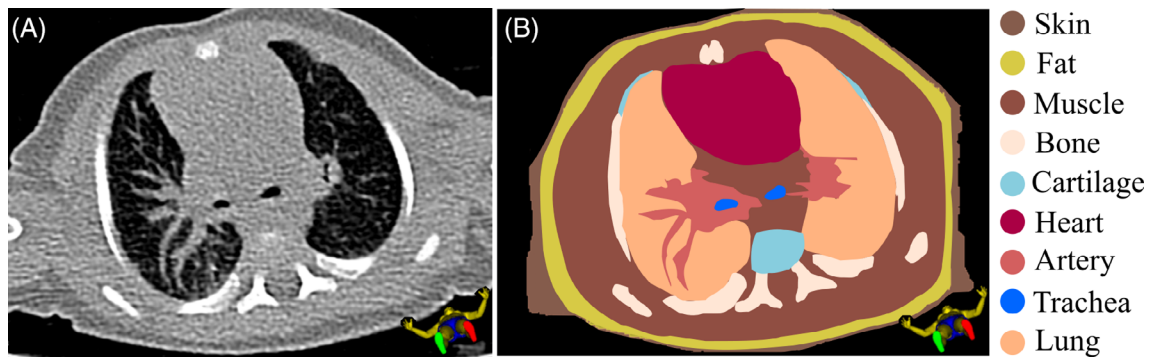


**FIGURE 1** (A) Axial plane slice from anonymized CT scan of a 3.58 kg infant born in gestational week 36 and (B) equivalent segmented slice where each colour highlights a specific tissue (see legend to the right)

from a computed tomography scan (CT) of a pre-term neonate. Each CT slice was segmented to distinguish nine different organs (skin, fat, muscle, bone, cartilage, heart, artery, trachea and lung). A set of optical properties, absorption and reduced scattering coefficients ( $\mu_a$  and  $\mu_s'$ ), were assigned to each organ, based on values available in literature (see Table 1). Finally, we modelled the intensity of light reaching detectors over the thorax with fixed endotracheal and dermal light sources; and evaluated how sensitive the signal would be to volume changes mimicking respiration.

## 2 | CONSTRUCTION OF THORACIC MODEL

### 2.1 | Anthropomorphic geometry

NIRFAST is a modelling and image reconstruction software, which uses Digital Imaging and Communications in Medicine (DICOM) images as input, to create computational models of biological tissue. These models preserve the anthropomorphic geometry of the segmented

organs and can be used to simulate near-infra-red (NIR) light propagation based on the finite element method (FEM) for a specific set of landmarks (source and detectors) defined by the user [39].

DICOM images from an anonymised CT scan of a 3.58 kg infant born in gestational week 36 were used to construct the computational 3D model of the thorax. The CT consisted of a stack of 367 cross sectional slices 0.625 mm thick. Each image had 512 × 512 pixels, with a pixel size of 0.356 mm in both directions. The CT scan was acquired after parental consent following the guidelines of the ethical approval ECM 4 (gg) 7 March 2018 from the Clinical Research Ethics Committee of the Cork Teaching Hospitals.

### 2.2 | Organ segmentation and creation of computational thorax

The 3D computational model of the thorax was constructed by means of NIRFAST, which allowed segmentation by direct drawing over the CT images. The organs conforming the computational thorax model were: skin,

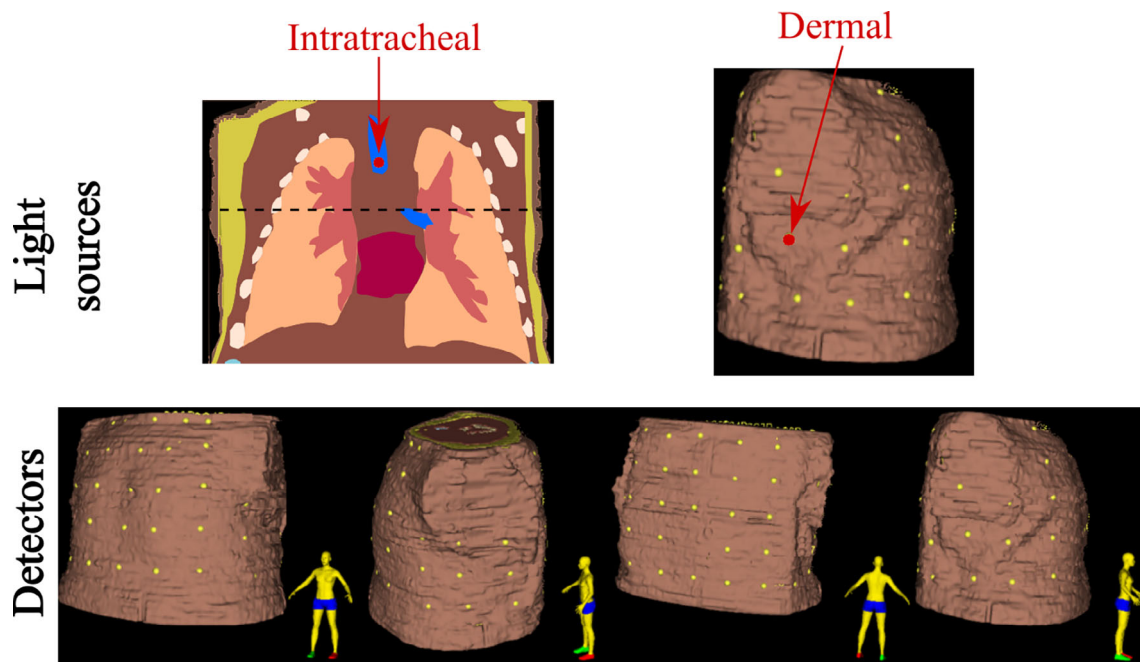


**FIGURE 2** Positions of source and detector landmarks in the computational models. In transmittance geometry, the source was located inside the trachea and in remittance geometry under the right armpit. A set of the 68 dermal detectors (yellow dots) was located around the thorax to model NIR light propagation. The dashed line corresponds to the axial plane in Figure 1

fat, muscle, bone, cartilage, heart, artery, trachea (including the primary bronchi) and lung (Figure 1). For segmentation purposes a different label was assigned to each organ present in the CT stack. The boundaries between organs were defined by differences in intensity levels of Hounsfield Units (HU), a quantitative scale used to describe tissue radio-density [40]. The segmentation tool “Grow from seeds” was used to create complete segmentation and avoid empty spaces within the model.

Each organ was considered optically homogeneous; small structures usually present in tissue like veins, collagen, etc. were absent in this model. The values of absorption and reduced scattering were taken from literature [10, 34, 39, 40]. The optical properties of trachea, primary bronchi and muscle were considered to be the same, as muscle is one of the main constituents of trachea [41]. Since the latest GASMAS prototype combines two diode lasers operating at 760 and 820 nm [30], those wavelengths were chosen for this study (Table 1).

To have a deeper understanding of the interaction of NIR light injected from the trachea or armpit with the lung and the surrounding organs, a set of landmarks (points which define a position in space) was placed in the model to represent two configurations, one with an endotracheal light source (transmittance geometry) and one with a dermal source placed under the right armpit

(remittance geometry). A group of detectors distributed over the torso was used for both configurations, as can be seen in Figure 2.

The segmentation and the landmarks were provided as input to execute the standard meshing routine of NIRFAST [39].

A three-dimensional (3D) mesh of the thorax was created to model the diffusion of NIR light. The mesh had 1 356 069 tetrahedral elements, 229 363 nodes and 69 landmarks in total.

### 2.3 | Respiration model

Lung volume measurements are essential for diagnosis and surveillance of respiratory diseases [42]. To understand the variation in the GASMAS signal linked to pulmonary volume changes during respiration, three sub-segments of the lung were created, as a simplified model of inflation stages between inspiration and expiration (Figure 3). The inspiratory reserve lung volume (IRV = 206 ml) was modelled assigning lung optical properties to all segments; the inspiratory lung volume (IV = 195 ml) assigning muscle optical properties to the most exterior segment; and the residual lung volume (RV = 137 ml) assigning lung optical properties to the inner segment and muscle optical properties to the external segments.

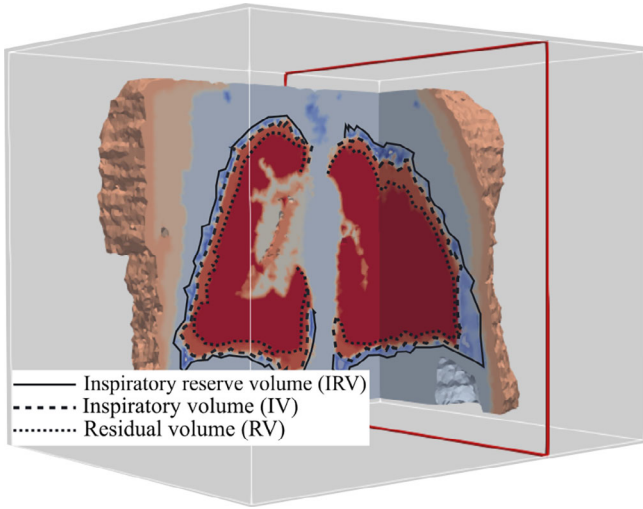


FIGURE 3 Computational model with lung sub-segments used to recreate the pulmonary volumes (IRV, IV and RV)

### 3 | MODELLING OF LIGHT PROPAGATION

#### 3.1 | Forward model and photon hitting density

At the utilised wavelengths, scattering interactions dominate over absorption ( $\mu_a \ll \mu_s'$ ) and the detectors were placed far from the source, therefore, the diffusion equation approximation was used to solve the NIR light propagation [34]. This was achieved through the forward model of NIRFAST for both 760 and 820 nm.

The primary output from the forward model is the light fluence rate  $\varphi(x, y, z)$  at each nodal point of the mesh. The absorption of light due to the presence of molecular  $O_2$  inside the alveoli can be computed, as the product of fluence rate in lung by the absorption of the gas. This absorption imprint of  $O_2$  is about  $10^{-4}$  weaker than that of the surrounding tissue and will not significantly change the value of fluence rate within the tissue [26].

The absorption imprint of the detected signal for any given position in the tissue is proportional to the photon hitting density ( $PHD$ ) [43]. The  $PHD$  describes the expected path length spent by photons at any given position when travelling between source and detector. It thereby shows the probability of a change in optical properties at a certain position to affect the measured signal [44]. The  $PHD$  was found by solving the forward model to estimate  $\varphi_S$  for a mesh node in a location  $(x, y, z)$  with the light injection point in the source ( $S$ ), followed by the calculation of  $\varphi_D$  assuming that the light injection point is now located in the position of the detector ( $D$ ) and multiplying both values:

$$PHD_{SD}(x, y, z) = \varphi_S(x, y, z) \cdot \varphi_D(x, y, z) \quad (2)$$

The total photon hitting density (TPHD) corresponds to the contribution from all nodes ( $n$ ) of the mesh. It is related to the total light intensity detected (see supplementary material), and does not provide information about the gas absorption in lung tissue.

$$TPHD_{SD} = \sum_{n_{\text{mesh}}} \varphi_S(x, y, z) \cdot \varphi_D(x, y, z) \quad (3)$$

Liao et al. introduced the concept of *sensitivity* ( $\sigma$ ) for GASMAS measurements, as the ratio between the sum of the  $PHD$  for nodal points allocated within the lung and the  $TPHD$  [26]. Source-detector configurations with high sensitivity are more likely to output a high gas absorption signal as the path length of light within the lung is a larger fraction of the total path length.

$$\sigma = \frac{\sum n_{\text{lung}} \varphi_S(x, y, z) \cdot \varphi_D(x, y, z)}{\sum n_{\text{mesh}} \varphi_S(x, y, z) \cdot \varphi_D(x, y, z)} \quad (4)$$

TPHD and  $\sigma$  were calculated at two wavelengths for the three different lung volumes: IRV, IV and RV, for two different configurations, one with endotracheal source and 68 detectors on the torso and with a dermal source under the right armpit and 67 detectors.

### 4 | RESULTS AND DISCUSSION

The interpolated values of the fluence rate for each nodal point in the lung when light is injected inside the trachea and under the armpit (dermal light source) are shown in Figure 4. The dermal source was located under the armpit in agreement with the translational investigation article published by Krite Svanberg et al. who found this geometry to be the most favourable to obtain gas absorption signal for a set of 21 full term infants [31]. These geometries are analysed throughout this study.

The placement of the intratracheal light source results in a gain of two orders of magnitude ( $\sim 1.6 \times 10^{-2}$ ) in light fluence rate in the lung. This means there will be more light interacting with the gas in the lung, while it tells little about how that absorption would be detectable at superficial locations around the thorax. To understand how placing an internal source could influence the detected signal in various positions over the torso, we revise next, the  $TPHD$  and  $\sigma$  for both configurations.

Equation 3 was computed for each of the 68 detectors with the source placed in the trachea of the computational model with optical properties at 760 and 820 nm. The interpolated values of  $TPHD$  were plotted for the

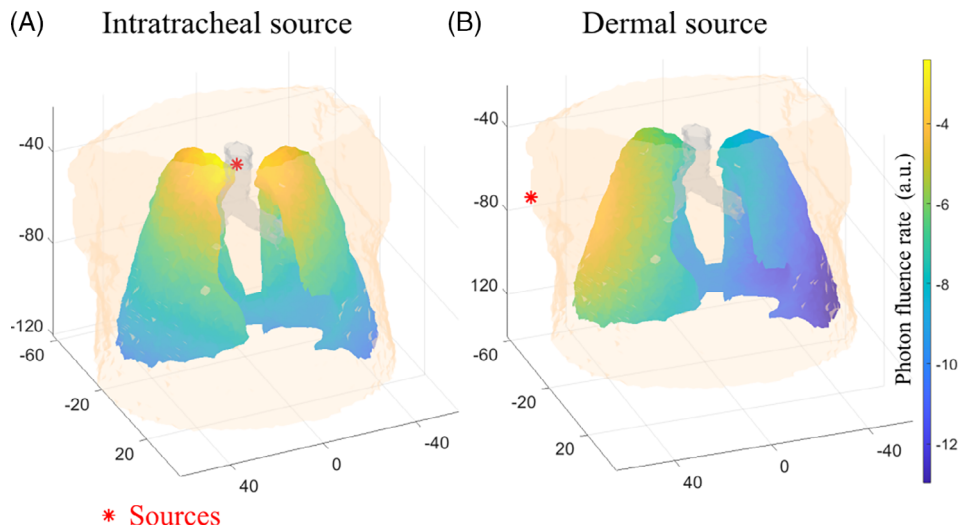


**FIGURE 4** Logarithmic maps of light fluence rate for the computational model with optical properties at 760 nm with a tracheal (A) and a dermal (B) light source, which position is represented by a red asterisk

different respiratory volumes in Figure 5A. The same calculation was performed with the dermal source. In that case the number of detectors was 67 and the landmark located in the trachea was discarded prior to the data interpolation which can be seen in Figure 5B.

The maximum value of *TPHD* is obtained for the remittance configuration (dermal source placed under the armpit). Detectors close to the source will detect high light signals and will therefore have high *TPHD*. We discuss the combined requirement of high *TPHD* and  $\sigma$  below.

For the intratracheal light source, the *TPHD* increases in the respiration phase as the lung volume decreases. This is most likely related to the higher light attenuation of lung tissue compared with muscle, which was used to replace the perimeters of lung tissue in the simulations, for the inspiratory and reserve lung volumes. We see the same tendency for the dermal source but less accentuated, most likely because less of the detected light will pass through the lung tissue for this geometry.

Comparing the two wavelengths (760 and 820 nm), the values of *TPHD* for the intratracheal source simulations do not differ much, meaning that both wavelengths are attenuated similarly when transmitted through the tissue. This is ideal for the assumptions of similar path lengths in the lung tissue for the two wavelengths, made to estimate  $O_2$  concentrations in the lung. In contrast, the light paths for the dermal source simulations are dominated by superficial tissue (skin, fat and muscle), and the light attenuation at 820 nm is lower for those tissues than at 760 nm, resulting in a higher *TPHD* for 820 nm compared with light at 760 nm.

To know how much of the light injected in the trachea and under the armpit would interact with the gas in the lung,  $\sigma$  was plotted for both configurations and all the pulmonary volumes in Figure 6. The regions of the

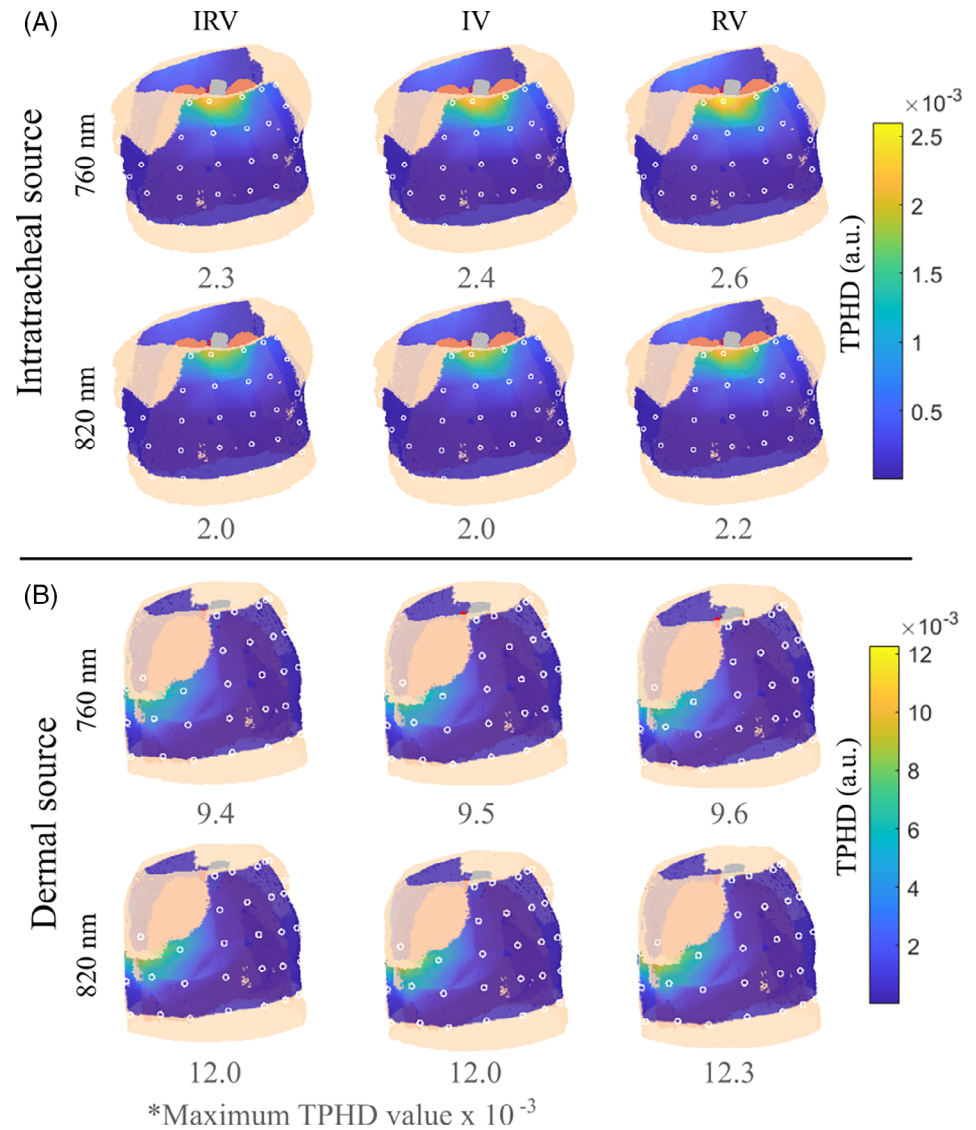
thorax with higher  $\sigma$  correspond to the configurations for which the light spent longer time interacting with lung tissue, which is correlated with higher gas absorption signals.

The  $\sigma$  maps for intratracheal source (Figure 6A) show that the percentage of the total path length spent in lung tissue is rather constant, independent on the detection configuration (slightly <1% of the total photon path is through lung tissue). A likely explanation is that the lung tissue is very close to the source and most of the path length is spent within the lung independently on the path the light takes through the tissue to reach the detectors. The pattern for the dermal source is very different (Figure 6B). For this configuration, the fraction of the path length spent in the lung tissue (deep into the body) is higher the further away from the source the detector is located. Comparing the two wavelengths, again  $\sigma$  differ more for the dermal than for the internal source, probably for same reason as discussed for the *TPHD*.

Figure 7A corresponds to transmittance geometry in which the source is placed in the trachea and the detectors over the thorax. In this case the light propagates towards the anterior ( $0^\circ$ – $180^\circ$ ) and posterior ( $180^\circ$ – $0^\circ$ ) sides of the thorax. The  $\sigma$  map overlaps at some angles with the *TPHD* lobes. This means it should be possible to obtain a position with both relatively high light transmission and gas sensitivity. Best detector position in this respect for this particular plane seems to be around  $30^\circ$ .

Figure 7B resembles the remittance geometry, in which the source (located under the armpit at  $330^\circ$ ) and detectors are placed over the thoracic wall. In this case, the light undergoes attenuation by the external tissues (i.e. bone, muscle, fat and skin) as light goes from the source to the lung and on the way back to the detector. This plot shows how the  $\sigma$  distribution is strong when the *TPHD* value is low and vice versa, meaning it is

**FIGURE 5** Interpolated *TPHD* for the respiratory volumes (IRV, IV and RV) at 760 and 820 nm with endotracheal (A) and dermal (B) light source with a set of detectors (circular markers) placed over the thorax. The numbers in grey indicate the maximum *TPHD* values within each case



unlikely to get both a strong light signal and sensitivity for the same source detector configuration. The optimal detection positions considering both sensitivity and light transmission is around  $300^\circ$ , corresponding to a measurable sensitivity and still a relatively high *TPHD*. This position relates well with the experimental findings reported in Ref [31].

The plots of Figure 7 are useful to identify optimum source-detector geometries. For example, the detectors shown in Table 2 will sense the highest signal carrying the absorption imprint of  $O_2$  gas inside the lung, at this specific coronal plane. The values of *TPHD* and  $\sigma$  for intratracheal and dermal source for those detectors are specified below:

Table 2, show that light delivered internally is more likely to carry as absorption imprints, associated with high  $\sigma$ . The results show that GASMAS has the potential to quantify changes in lung volume, which could be correlated with the alveolar status of lung

tissue. And, it could be possible to perform continuous bedside measurement of pulmonary volumes in neonates. This represents an advantage compared with current methods such as radiography, gas dilution (requires the infant to remain quiet for at least 10 min) and plethysmography (not suitable for bedside measurements or assessment in very small infants) [45]. Electrical impedance tomography can be used to monitor changes in regional ventilation and lung volume in infants, but lacks of information about the alveolar gas content [46].

It should be noted that in this study the light sources were placed in a fixed position and a different placement would alter the light distribution and to some extent the conclusions. However, these results are in agreement with the experimental studies performed in Biophotonics@Tyndall in which the optical properties and structure of tissue from the respiratory zone were modelled in an optical phantom, that enabled benchtop

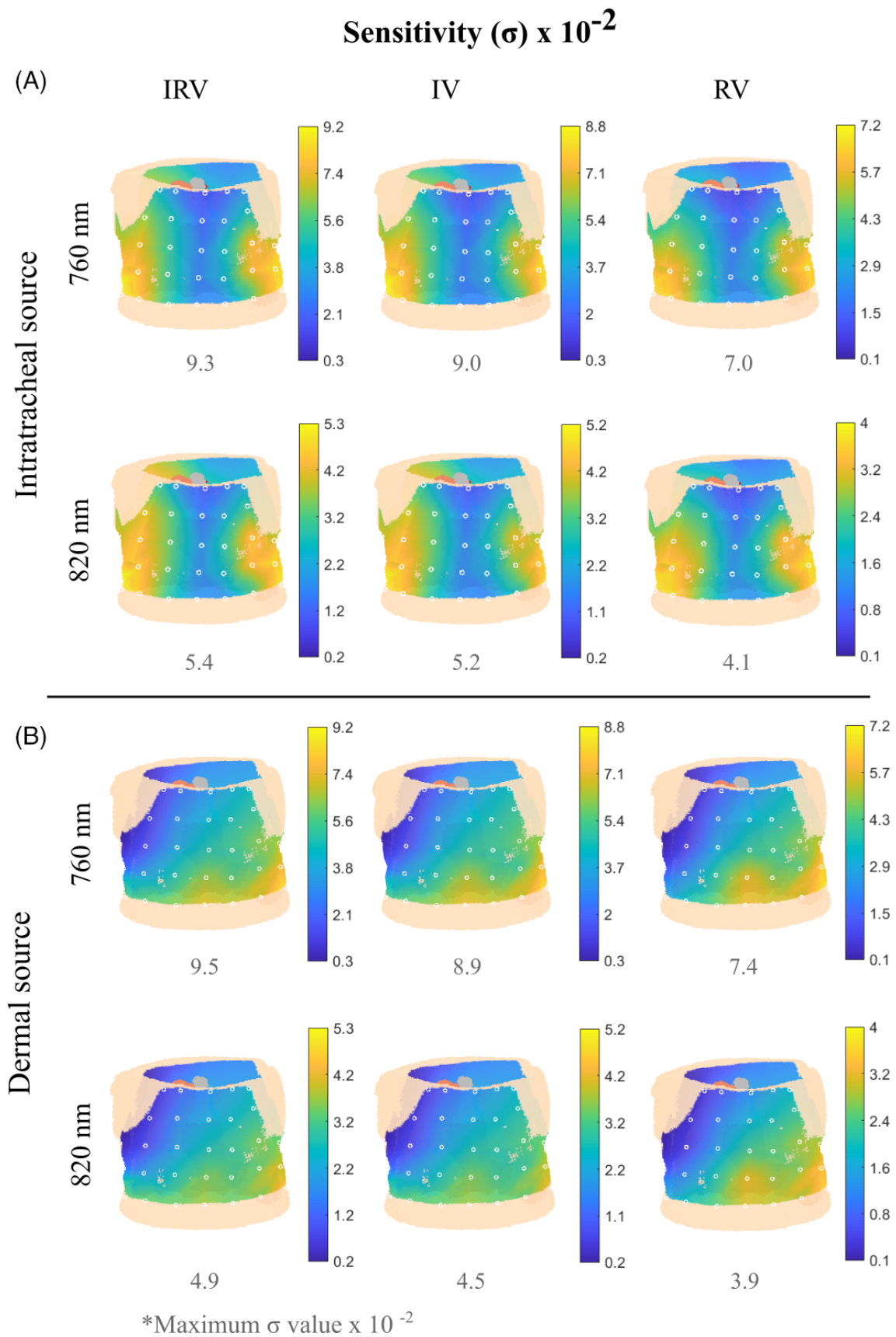


**FIGURE 6** Sensitivity ( $\sigma$ ) plots for the respiratory volumes (IRV, IV and RV) at 760 nm (top row) and 820 nm (bottom row) with endotracheal (A) and dermal (B) light source with a set of detectors (circular markers) placed over the thorax. The numbers in grey indicate the maximum  $\sigma$  values

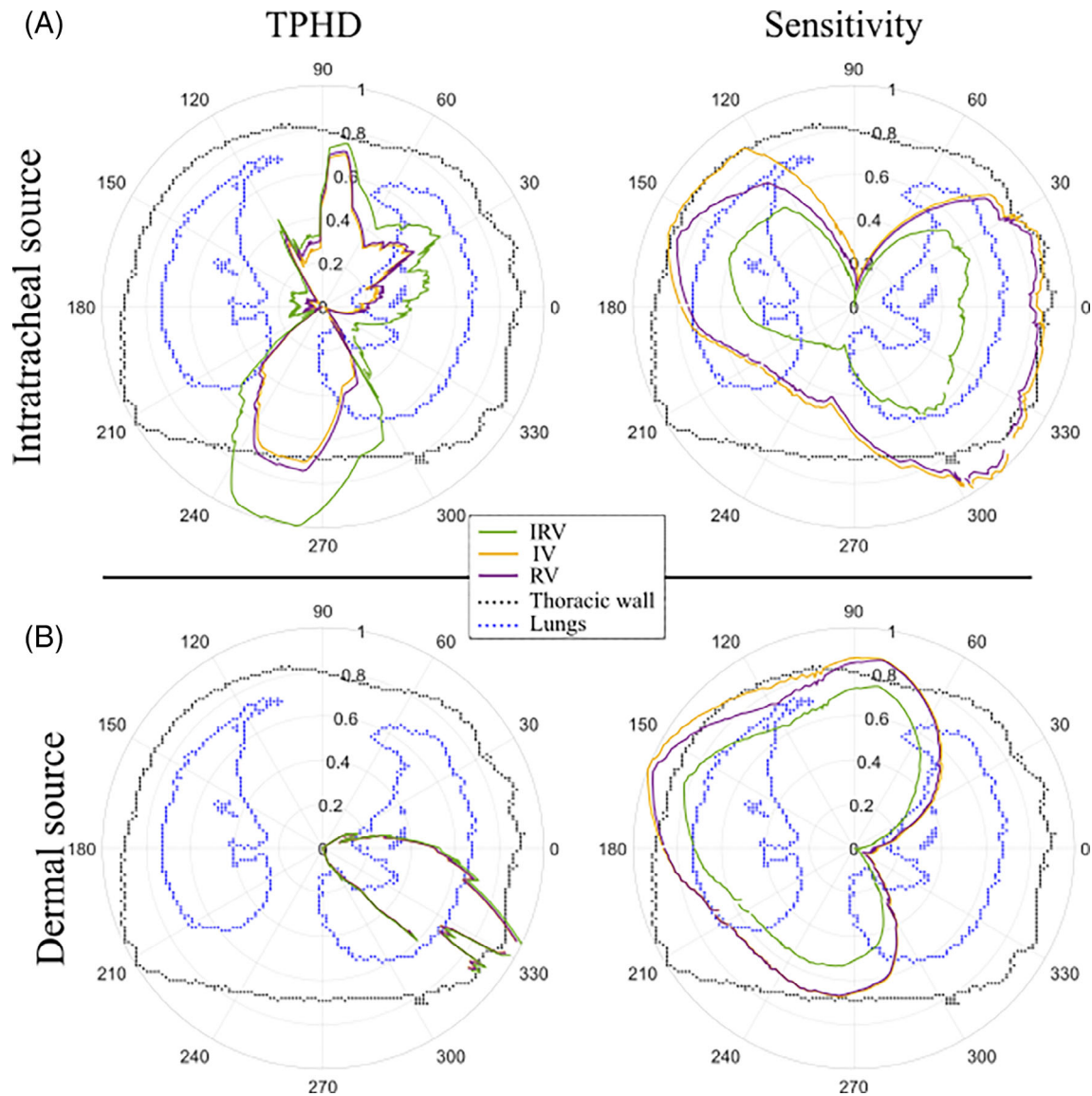


**FIGURE 7** The normalised polar plot of the  $TPHD$  and  $\sigma$  values for the intratracheal and dermal sources at 760 nm. The coronal plane (vertical plane dividing the body into anterior and posterior parts) is signed with the dashed line in Figure 2

measurements of changes in gas volume with a GASMAS system in transmittance geometry [47]. And the gain in detected signal carrying information of gas absorption (photons reaching the detector after interacting with lung tissue), associated with the placement of an endotracheal light source compared with the dermal source, is in agreement with the results from Krite Svanberg et al. who analysed  $O_2$  and  $H_2O$  absorption signals in five mechanically ventilated piglets with a probe delivering light externally, on the skin and internally, through the oesophagus [30]. In the same study, the authors found a weak or non-existent  $H_2O$  vapour signal when using the dermal light source, and as a consequence, the determination of  $O_2$  concentration was not achieved. The low  $\sigma$  for the dermal source at 820 nm exhibited in Figure 6B confirms that for this configuration, a small amount of light reaches the

lung and the associated GASMAS signal would be non-existent or low.

Preterm infants with severe RDS often need intubation for invasive mechanical ventilation due to respiratory failure. A naso-gastric tube is inserted in almost all preterm infants for feeding purposes. Placing a light source in the trachea or the oesophagus would be feasible, and it will still be “noninvasive”, since the light source would be placed in the trachea through an already existing tube. The stronger signals, would further allow to reduce the measurement times to permit recordings of the  $O_2$  levels in the lung as a function of phase in the respiration cycle. However, the main aim of GASMAS translated into respiratory health-care, is a noninvasive assessment of lung function, and the internal light source should be used just if the infant is already intubated. The

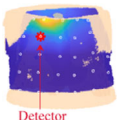
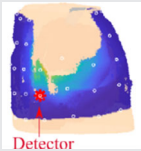
Source- detector configuration		Respiratory volume	TPHD $\times 10^{-4}$	$\sigma \times 10^{-2}$
 Intratracheal source	760	IRV	5.2	4.7
		IV	5.4	4.5
		RV	6.2	3.1
	820	IRV	4.0	3.2
		IV	4.2	3.1
		RV	5.0	2.1
 Dermal source	760	IRV	13	1.0
		IV	13	0.9
		RV	14	0.4
	820	IRV	14	0.6
		IV	15	0.5
		RV	16	0.2

TABLE 2 TPHD and  $\sigma$  values for the different respiratory volumes, with the best source detector configurations in Figure 7

localization of a near- infra-red light fibre inside the respiratory or potentially naso-gastric feeding tube, could be prototyped and evaluated.

The enhancement of sophisticated neonatal intensive care is increasing the viability of extremely preterm babies. However, prolonged intubation in low birthweight neonates is associated with risk of infection and higher morbidity [48]. The clinical translation of GASMAS technique can potentially be of help in aiding physicians to diagnose and continuously monitor the respiratory function of pre-term infants and their response to oxygen and surfactant administration [49]. As a noninvasive technique it also could develop as a tool to optimise time for extubation (withdrawal of the endotracheal tube) and contribute to the current need of improving new-born medical care [2].

## 5 | CONCLUSION

An anthropomorphic computational model of the thorax of a neonate with nine main organs (skin, fat, muscle, bone, cartilage, heart, artery, trachea and lung) was created. The model was used to simulate light propagation at 760 and 820 nm wavelength, for two different light-source detector configurations (remittance and transmittance geometries) during respiration.

The sensitivity maps showed that the placement of an endotracheal light source would improve the assessment of the pulmonary lobes, as light exhibits less attenuation and distributes evenly in the lung.

The variations in TPHD and  $\sigma$  associated to changes in pulmonary volume suggest that GASMAS can be used to assess continuously lung volumes during respiration.

The results from this study are in agreement with the experimental studies conducted by Krite Svanberg et al. in a group of mechanically ventilated piglets; our numerical model could be further used to analyse different source-detector configurations and assist in the planning of clinical protocols to advance the clinical translation of GASMAS as a complementary tool to improve the respiratory healthcare in neonates.

## ACKNOWLEDGMENTS

The authors like to thank Monisha Chakravarty for helping with segmentation. The research leading to these results was funded by Science Foundation Ireland project no. SFI/15/RP/2828. Open access funding provided by IReL.

## CONFLICTS OF INTEREST

The authors declare no conflict of interest.

## AUTHOR CONTRIBUTIONS

Andrea Pacheco was involved in conceptualization, investigation and writing—original draft; Baptiste Jayet was involved in conceptualization, investigation and writing—plots; Emilie Krite Svanberg, Hamid Dehghani, Eugene Dempsey and Stefan Andersson-Engels were involved in conceptualization, writing—review and editing and Stefan Andersson-Engels was involved in supervision and project management.

## DATA AVAILABILITY STATEMENT

The data from the discrete 3D mesh of the thorax of the neonate are openly available at the public repository <https://doi.org/10.5281/zenodo.4916862>. The scripts that support the findings of this study are openly

available at the public repository <https://doi.org/10.5281/zenodo.5996855>.

## ORCID

Andrea Pacheco  <https://orcid.org/0000-0002-1856-4731>

## REFERENCES

- [1] S. Beck, D. Wojdyla, L. Say, A. Pilar Bertran, M. Meraldi, J. Harris Requejo, C. Rubens, R. Menon, P. Van Look, *Bull World Health Org* **2010**, 88, 31.
- [2] H. Blencowe, S. Cousens, D. Chou, M. Oestergaard, L. Say, A.-B. Moller, M. Kinney, J. Lawn, *Reprod Health* **2013**, 10, S2.
- [3] T. J. M. Moss, *Proc Aust Physiol Soc* **2005**, 36, 23.
- [4] P. O. Kero, E. O. Mikinen, *Eur. J. Pediatr.* **1979**, 130, 271.
- [5] C. L. Hermansen, A. Mahajan, L. G. Hospital, *Am. Fam. Physician* **2007**, 76, 987.
- [6] R. Soll, C. J. Morley, *Cochrane Database of Systematic Reviews (Ed.: The Cochrane Collaboration)*, John Wiley & Sons, Ltd, Chichester, UK **2001**, CD000510.
- [7] K. N. Farrow, P. Fliman, R. H. Steinhorn, *Semin. Perinatol.* **2005**, 29, 8.
- [8] M. Sjöholm, G. Somesfalean, J. Alnis, S. Andersson-Engels, S. Svanberg, *Opt. Lett.* **2001**, 26, 16.
- [9] I. E. Gordon, L. S. Rothman, C. Hill, R. V. Kochanov, Y. Tan, P. F. Bernath, M. Birk, V. Boudon, A. Campargue, K. V. Chance, B. J. Drouin, J.-M. Flaud, R. R. Gamache, J. T. Hodges, D. Jacquemart, V. I. Perevalov, A. Perrin, K. P. Shine, M.-A. H. Smith, J. Tennyson, G. C. Toon, H. Tran, V. G. Tyuterev, A. Barbe, A. G. Császár, V. M. Devi, T. Furtenbacher, J. J. Harrison, J.-M. Hartmann, A. Jolly, T. J. Johnson, T. Karman, I. Kleiner, A. A. Kyuberis, J. Loos, O. M. Lyulin, S. T. Massie, S. N. Mikhailenko, N. Moazzen-Ahmadi, H. S. P. Müller, O. V. Naumenko, A. V. Nikitin, O. L. Polyansky, M. Rey, M. Rotger, S. W. Sharpe, K. Sung, E. Starikova, S. A. Tashkun, J. V. Auwera, G. Wagner, J. Wilzewski, P. Wcisło, S. Yu, E. J. Zak, *J Quant Spectrosc Radiat Transf* **2017**, 203, 3.
- [10] S. L. Jacques, *Phys. Med. Biol.* **2013**, 58, R37.
- [11] J. Alnis, B. Anderson, M. Sjöholm, G. Somesfalean, S. Svanberg, *Appl Phys B* **2003**, 77, 691.
- [12] T. Svensson, E. Alerstam, J. Johansson, S. Andersson-Engels, *Opt. Lett.* **2010**, 35, 1740.
- [13] P. Lundin, L. Cocola, M. Lewander, A. Olsson, S. Svanberg, *J. Food Eng.* **2012**, 111, 612.
- [14] T. Svensson, E. Adolfsson, M. Burresti, R. Savo, C. T. Xu, D. S. Wiersma, S. Svanberg, *Appl Phys B* **2013**, 110, 147.
- [15] L. Mei, G. Somesfalean, S. Svanberg, *Sensors* **2014**, 14, 3871.
- [16] M. Lewander, Z. Guan, K. Svanberg, S. Svanberg, T. Svensson, *Opt Express* **2009**, 17, 10849.
- [17] L. Persson, K. Svanberg, S. Svanberg, *Appl Phys B* **2006**, 82, 313.
- [18] J. Huang, H. Zhang, T. Li, H. Lin, K. Svanberg, S. Svanberg, *J. Biophotonics* **2015**, 8, 985.
- [19] L. Hu, W. Li, H. Lin, Y. Li, H. Zhang, K. Svanberg, S. Svanberg, *J. Biophotonics* **2019**, 12, e201800305.
- [20] D. Chen, W. Li, W. He, H. Zhang, Q. Zhang, H. Lin, S. Svanberg, K. Svanberg, P. Chen, *J. Biomed. Opt.* **2019**, 24, 1.
- [21] M. Lewander, A. Bruzelius, S. Svanberg, K. Svanberg, V. Fellman, *J. Biomed. Opt.* **2011**, 16, 127002.
- [22] P. Lundin, E. K. Svanberg, L. Cocola, M. L. Xu, G. Somesfalean, S. Andersson-Engels, J. Jahr, V. Fellman, K. Svanberg, S. Svanberg, *J. Biomed. Opt.* **2013**, 18, 127005.
- [23] W. Rosa Ed., *A New Era in Global Health*, Springer Publishing Company, New York, NY **2017**.
- [24] A. L. Buck, *J. Appl. Meteorol.* **1981**, 20, 1527.
- [25] D. F. Swinehart, *J. Chem. Educ.* **1962**, 39, 3.
- [26] P. Liao, J. Larsson, E. K. Svanberg, P. Lundin, J. Swartling, M. L. Xu, J. Bood, S. Andersson-Engels, *J. Biophotonics* **2018**, 11, 7.
- [27] J. Larsson, P. Liao, P. Lundin, E. Krite Svanberg, J. Swartling, M. Lewander Xu, J. Bood, S. Andersson-Engels, *J. Biophotonics* **2018**, 11, e201700097.
- [28] J. Larsson, D. Leander, M. Lewander Xu, V. Fellman, J. Bood, E. Krite Svanberg, *J. Biophotonics* **2019**, 12, e201800350. <https://doi.org/10.1002/jbio.201800350>.
- [29] A. Pacheco, H. Li, M. Chakravarty, S. K. V. Sekar, S. Andersson-Engels, *J. Biomed. Opt.* **2020**, 25, 25. <https://doi.org/10.1117/1.JBO.25.11.115001>.
- [30] E. K. Svanberg, J. Larsson, M. Rasmussen, M. Larsson, D. Leander, S. Bergsten, J. Bood, G. Greisen, V. Fellman, *Pediatr. Res.* **2020**, 89, 823. <https://doi.org/10.1038/s41390-020-0971-x>.
- [31] E. K. Svanberg, P. Lundin, M. Larsson, J. Åkeson, K. Svanberg, S. Svanberg, S. Andersson-Engels, V. Fellman, *Pediatr. Res.* **2016**, 79, 621.
- [32] P. Lundin, E. K. Svanberg, L. Cocola, M. Lewander, S. Andersson-Engels, J. Jahr, V. Fellman, K. Svanberg, S. Svanberg, in *Proc. SPIE 8229, Optical Diagnostics and Sensing XII: Toward Point-of-Care Diagnostics; and Design and Performance Validation of Phantoms Used in Conjunction with Optical Measurement of Tissue IV* (Eds: R. J. Nordstrom, G. L. Coté), SPIE BiOS, San Francisco, CA **2012**, 822903. <https://doi.org/10.1117/12.907464>.
- [33] E. K. Svanberg, S. Svanberg, Device and technique for internal illumination for human gas monitoring., n.d., CN107923847A.
- [34] H. Dehghani, M. E. Eames, P. K. Yalavarthy, S. C. Davis, S. Srinivasan, C. M. Carpenter, B. W. Pogue, K. D. Paulsen, *Commun. Numer. Methods Eng.* **2009**, 25, 711.
- [35] N. Choudhury, R. Samatham, S. L. Jacques, in *Proc. SPIE 7548, Photonic Therapeutics and Diagnostics VI*, 75480G, **2010**. <https://doi.org/10.1117/12.842648>.
- [36] R. L. P. van Veen, H. J. C. M. Sterenborg, A. Pifferi, A. Torricelli, R. Cubeddu, *Biomedical topical meeting*, OSA, Optica Publishing Group, Miami Beach, FL **2004**, p. SF4.
- [37] R. Re, I. Pirovano, D. Contini, L. Spinelli, A. Torricelli, *Sensors* **2018**, 18, 264.
- [38] D. W. Ebert, C. Roberts, S. K. Farrar, W. M. Johnston, A. S. Litsky, A. L. Bertone, *J. Biomed. Opt.* **1998**, 3, 326.
- [39] M. Jermyn, H. Ghadyani, M. A. Mastanduno, W. Turner, S. C. Davis, H. Dehghani, B. W. Pogue, *J. Biomed. Opt.* **2013**, 18, 086007.
- [40] M. Mahesh, *Radiographics* **2002**, 22, 14.
- [41] B. E. M. Brand-Saberi, T. Schäfer, *Thorac. Surg. Clin.* **2014**, 24, 1.
- [42] M. F. Lutfi, *Multidiscip. Respir. Med.* **2017**, 12, 3.
- [43] J. C. Schotland, J. C. Haselgrove, J. S. Leigh, *Appl. Optics* **1993**, 32, 448.
- [44] S. R. Arridge, *Appl. Optics* **1995**, 34, 7395.

- [45] G. Hülskamp, J. J. Pillow, J. Dinger, J. Stocks, *Pediatr. Pulmonol.* **2006**, *41*, 1.
- [46] I. Chatziioannidis, T. Samaras, N. Nikolaidis, *Hippokratia* **2011**, *15*, 211.
- [47] A. Pacheco, K. Grygoryev, W. Messina, S. Andersson-Engels, *J. Biomed. Opt.* **2021**, *27*, 27. <https://doi.org/10.1117/1.JBO.27.7.074707>.
- [48] D. Holleman-Duray, D. Kaupie, M. G. Weiss, *J. Perinatol.* **2007**, *27*, 776.
- [49] A. Pacheco, E. Dempsey, S. Andersson-Engels, *Asian J Basic Sci Res* **2020**, *9*, 251.

## SUPPORTING INFORMATION

Additional supporting information may be found in the online version of the article at the publisher's website.

**How to cite this article:** A. Pacheco, B. Jayet, E. K. Svanberg, H. Dehghani, E. Dempsey, S. Andersson-Engels, *J. Biophotonics* **2022**, e202200041. <https://doi.org/10.1002/jbio.202200041>